

RESEARCH ARTICLE

Open Access



# A personal acquisition time regimen of $^{68}\text{Ga}$ -DOTATATE total-body PET/CT in patients with neuroendocrine tumor (NET): a feasibility study

Jie Xiao<sup>1,2,3†</sup>, Haojun Yu<sup>1,2,3†</sup>, Xiuli Sui<sup>1,2,3</sup>, Guobing Liu<sup>1,2,3</sup>, Yanyan Cao<sup>1,2,3</sup>, Zhao Yanzhao<sup>1,2,3</sup>, Yiqiu Zhang<sup>1,2,3,4</sup>, Pengcheng Hu<sup>1,2,3</sup>, Dengfeng Cheng<sup>1,2,3\*</sup> and Hongcheng Shi<sup>1,2,3,4\*</sup>

## Abstract

**Background:** The injection activity of tracer, acquisition time, patient-specific photon attenuation, and large body mass, can influence on image quality. Fixed acquisition time and body mass related injection activity in clinical practice results in a large difference in image quality. Thus, this study proposes a patient-specific acquisition time regimen of  $^{68}\text{Ga}$ -DOTATATE total-body positron emission tomography-computed tomography (PET/CT) to counteract the influence of body mass (BM, kg) on image quality, and acquire an acceptable and constant image of patients with neuroendocrine tumors (NETs).

**Methods:** The development cohort consisting of 19 consecutive patients with full activity (88.7–204.9 MBq,  $2.0 \pm 0.1$  MBq/kg) was to establish the acquisition time regimen. The liver SNR (signal-to-noise ratio,  $\text{SNR}_L$ ) was normalized ( $\text{SNR}_{\text{norm}}$ ) by the product of injected activity (MBq) and acquisition time (min). Fitting of  $\text{SNR}_{\text{norm}}$  against body mass (BM, kg) in linear correlation was performed. Subjective assessment of image quality was performed using a 5-point Likert scale to determine the acceptable threshold of  $\text{SNR}_L$ , and an optimized acquisition regimen based on BM was proposed, and validated its feasibility through the validation cohort of 57 consecutive NET patients with half activity ( $66.9 \pm 11.3$  MBq,  $1.0 \pm 0.1$  MBq/kg) and a fixed acquisition time regimen.

**Results:** The linear correlation ( $R^2 = 0.63$ ) between  $\text{SNR}_{\text{norm}}$  and BM (kg) was  $\text{SNR}_{\text{norm}} = -0.01 \cdot \text{BM} + 1.50$ . The threshold  $\text{SNR}_L$  of acceptable image quality was 11.2. The patient-specific variable acquisition time regimen was determined as:  $t$  (min) =  $125.4 / (\text{injective activity}) \cdot (-0.01 \cdot \text{BM} + 1.50)^2$ . Based on that proposed regimen, the average acquisition time for acceptable image quality in the validation cohort was  $2.99 \pm 0.91$  min, ranging from 2.18 to 6.35 min, which was reduced by 36.50%~78.20% compared with the fixed acquisition time of 10 min. Subjective evaluation showed that acceptable image quality could be obtained at 3.00 min in the validation group, with an average subjective score of  $3.44 \pm 0.53$  ( $\kappa = 0.97$ , 95% CI: 0.96~0.98). Bland–Altman analysis revealed good agreement between the proposed regimen and the fixed acquisition time cohort.

†Jie Xiao and Haojun Yu contributed equally to this work.

\*Correspondence: Cheng.dengfeng@zs-hospital.sh.cn; Shi.hongcheng@zs-hospital.sh.cn

<sup>1</sup> Department of Nuclear Medicine, Zhongshan Hospital, Fudan University, 180 Fenglin Road, 200032 Shanghai, P.R. China  
Full list of author information is available at the end of the article



© The Author(s) 2022. **Open Access** This article is licensed under a Creative Commons Attribution 4.0 International License, which permits use, sharing, adaptation, distribution and reproduction in any medium or format, as long as you give appropriate credit to the original author(s) and the source, provide a link to the Creative Commons licence, and indicate if changes were made. The images or other third party material in this article are included in the article's Creative Commons licence, unless indicated otherwise in a credit line to the material. If material is not included in the article's Creative Commons licence and your intended use is not permitted by statutory regulation or exceeds the permitted use, you will need to obtain permission directly from the copyright holder. To view a copy of this licence, visit <http://creativecommons.org/licenses/by/4.0/>. The Creative Commons Public Domain Dedication waiver (<http://creativecommons.org/publicdomain/zero/1.0/>) applies to the data made available in this article, unless otherwise stated in a credit line to the data.

**Conclusion:** A patient-specific acquisition time regimen was proposed in NET patients in development cohort and validated its feasibility in patients with NETs in validation cohort by  $^{68}\text{Ga}$ -DOTATATE total-body PET/CT imaging. Based on the proposed regimen, the homogenous image quality with optimal acquisition time was available independent of body mass.

**Keywords:** Image quality, Variable acquisition time regimen, Total-body PET,  $^{68}\text{Ga}$ -DOTATATE, PET/CT imaging

## Background

Neuroendocrine tumors (NETs) comprise a heterogeneous group of tumors originating from neuroendocrine cells and involving multiple organs, particularly the gastrointestinal tract and lungs [1]. Marked expression of somatostatin receptor (SSTR) subtypes (SSTR1-SSTR5) is the main feature of NET cells, with overexpression of SSTR2 [2]. PET imaging with  $^{68}\text{Ga}$ -DOTA-Tyr3-Thr8-octreotide ( $^{68}\text{Ga}$ -DOTATATE) has higher affinity for SSTR-positive tissue ( $0.2 \pm 0.04$  nM) than other SSTR imaging agents [3, 4].

Total-body PET detector crystals with a size of  $2.76 \times 2.76 \times 18.0$  mm<sup>3</sup> coupled to silicon photomultipliers (SIPMs) shows ultrahigh sensitivity and spatial resolution [5]. Recently, a series of studies reported that low injection activity of  $^{18}\text{F}$ -FDG or a shorter scan time of total-body PET/CT imaging could still be feasible for good image quality [6–9]. Additionally, influence factors of image quality were varied and complicated, such as PET equipment, activity of the tracer, acquisition time, and patient-specific photon attenuation, particularly for large body mass. In terms of conventional PET equipment, increasing injection activity and prolonging acquisition time to some extent might improve image quality. However, the probability of radiation-related injury and later-occurring effects, and the possibility of motion artifacts inevitably increased [10]. As such, fixed acquisition time in clinical practice may result in significant differences in image quality between patients with varied body mass.

Regarding constant and acceptable image quality, we previously investigated the influence of patient size on image quality, and proposed a dose regimen based on body mass index (BMI, kg/m<sup>2</sup>), demonstrating the feasibility of constant image quality for  $^{18}\text{F}$ -FDG total-body PET/CT [11]. In addition, adjusting the duration time per bed based on scanner sensitivity and patient-specific attenuation might acquire uniform image noise or homogenous image [12]. For  $^{68}\text{Ga}$ -DOTATATE imaging, body mass (BM) was regarded as the strongest correlation with image quality [13]. However, the injection activity and acquisition time of  $^{68}\text{Ga}$ -DOTATATE vary in the literature, with reduced comparability of image quality between different studies. The regimen of a variable-acquisition time of  $^{68}\text{Ga}$ -DOTATATE PET/CT for an

acceptable and constant image has not been investigated thus far. Therefore, the aim of the present study was to propose a variable acquisition time regimen to balance the influence of scanners and BM and to obtain homogenous image quality for patients with NETs.

## Methods

### Patient population

All patient information was obtained in accordance with institutional ethical standards, and all included patients waived written informed consent prior to recruitment into the study (Approval No. B2020-186R). In total, 101 consecutive patients diagnosed with or suspected of having NET who underwent  $^{68}\text{Ga}$ -DOTATATE total-body PET/CT from September 2020 to January 2021 in our center were retrospectively analyzed. Prior to injection, patients were randomly and blindly (patient and image-evaluation physician) divided into the two cohorts: the development cohorts and the validation cohort. The development cohort was the full-activity group with activity of  $2.0 \pm 0.1$  MBq/kg (88.7–204.9 MBq), and the development cohort was the low-activity group with activity of  $1.0 \pm 0.1$  MBq/kg (66.9 ± 11.3 MBq). Figure 1 shows the process of patient recruitment, including the inclusion and exclusion criteria. We exclude patients with continuous treatment with Octreotide ( $N=6$ ), treatment with high intensity focused ultrasound in liver within 1 week ( $N=1$ ), diffused lesions in liver, fatty liver, and cirrhosis ( $N=5$ ). Finally, 48 underwent surgical resection as initial treatment, and the other 28 underwent biopsy. All cases were graded according to AJCC 2017 [14]; the remaining portion of the lesion without pathological examination was proven to be NET according to follow-up clinical and imaging data. All participants included in this study followed the standard procedures established by our center.

### $^{68}\text{Ga}$ -DOTATATE PET/CT imaging and image reconstruction

$^{68}\text{Ga}$ -DOTATATE was synthesized in-house according to a method previously described in the literature [15]. None of the participants needed to fast before tracer injection. Imaging was acquired using the following steps, as illustrated in Supplement Fig. 1: (1) Low radiation dose CT was performed before PET imaging for attenuation correction with a voltage of 120 kV

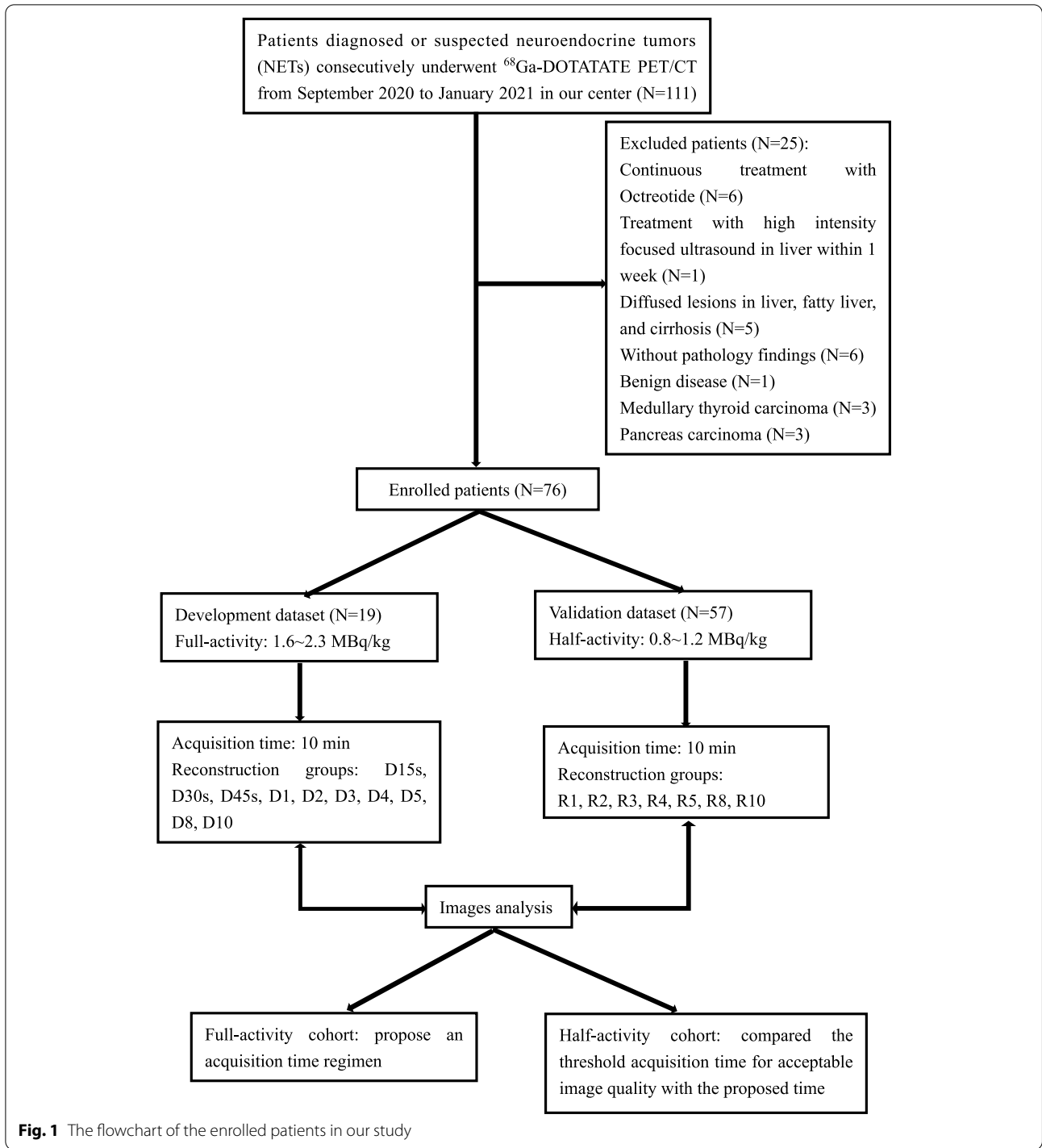


**Fig. 1** The flowchart of the enrolled patients in our study

and a current of 10 mA. (2) Images were acquired for 10 min in 3D-list mode for 50 min post injection of <sup>68</sup> Ga-DOTATATE. All imaging was performed on uEXPLORER (United Imaging Healthcare, Shanghai, China) PET/CT with an axial FOV of 194 cm. (3) The tube voltage of diagnostic CT was 120 kV, and the tube

current modulation technology was utilized to minimize the radiation dose.

Injection activity followed the BM-based linear dose regimen in both cohorts. Table 1 summarizes the current scanning and reconstruction protocol. In the development cohort, the images were further split into

**Table 1** Current scanning and reconstruction protocol

Characteristics	Parameters
Scanner	uEXPLORER total-body PET/CT
Crystal, Size [mm <sup>3</sup> ]	LYSO, 2.76 × 2.76 × 18.0
Amplifier	SiPM
Timing resolution (ps)	430
Axial FOV [cm]	194
Injected dose (MBq/Kg)	Full-activity: 1.6–2.3; Half-activity: 0.8–1.2
Uptake time (min)	50
Acquisition time (min)	10
Attenuation correction	ACCT
Reconstruction methods	PSF + TOF + 3D-OSEM
Reconstruction times (min)	Half-activity (30 s, 45 s, 60 s), All dataset: 1, 2, 3, 4, 5, 8, 10 min
Iterations/subsets	3/20
Slice thickness [mm]	1.443
Matrix	192 × 192

FOV Field of view, LYSO Lutetiumyttrium oxyorthosilicate, SiPM Silicon photomultiplier, ACCT Attenuation correction computed tomography, PSF Point function modeling, TOF Time of fly, 3D-OSEM 3D list-mode ordered-subset expectation maximization algorithm

reconstruction groups of 15 s, 30 s, 45 s, 1 min, 2 min, 3 min, 4 min, 5 min, 8 min and 10 min, which were defined as D15s, D30s, D45s, D1, D2, D3, D4, D5, R8 and D10, respectively. In the validation cohort, the images were split into reconstruction groups of 1 min, 2 min, 3 min, 4 min, 5 min, 8 min and 10 min, which were defined as R1, R2, R3, R4, R5, R8 and R10, respectively. PET images were reconstructed using the 3D list-mode ordered-subset expectation maximization algorithm (3D-OSEM) combined with the following parameters: time of flight and point spread function modeling (TOF-PSF), 3 iterations with 20 subsets, matrix of 192 × 192 and slice thickness of 1.443 mm, and full width at half-maximum (FWHM) of the Gaussian filter function of 3 mm.

### Qualitative image analysis

The image quality of all 76 patients was independently evaluated by two nuclear medicine physicians (Jie Xiao with 3 years and Xiuli Sui with 2 years of experience in interpreting PET images); to minimize bias, they were blinded to the patient's medical history, injection activity and the reconstruction time. Two reading sessions separated by 3–4 weeks were performed by each reader. Before interpreting the images, the two readers performed consistency training using standard images formulated according to the rule of 5-points Likert scale; the intra- and inter-reader agreement of these standard images should have kappa values over 0.85 (Table S1). The image

quality was scored from 3 perspectives: the overall impression of the image quality, the image noise, and the lesion detectability. Score were based on a 5-point Likert scale, as follows: Score 1, image with non-diagnostic quality, excessive noise, or unfavorable lesion contrast; Score 2, acceptable image but with sub-optimal noise and lesion depiction leading to impaired diagnostic confidence; Score 3, image with quality equivalent to those used in clinical practice; Score 4, image with quality superior to the average image quality; Score 5, image with excellent quality, optimal noise, sharp lesion depiction, and free of artifact, providing diagnosis with full confidence [11]. A score of 3 was deemed as acceptable image quality in routine clinical practice in our center. IN the event of large evaluation differences between the readers, the images were discussed in a consensus meeting.

### Semiquantitative image quality

To measure background uptake of the liver, an ROI (region of interest) with a diameter of 20 mm was drawn in the right lobe of the liver at the portal vein bifurcation section, avoiding any lesions and large vessels for measuring background uptake of the liver. The ROI of the lesion was placed in the highest pixel value on the transverse view, and an overall maximum of five lesions per patient was measured in multiple lesions. For objective evaluation of image quality, the signal-to-noise ratio of the liver ( $SNR_L$ ) was used and calculated by dividing the liver  $SUV_{mean}$  by its SD (Eq. 1) [16].

$$SNR_L = \frac{SUV_{mean}}{SD} \quad (1)$$

The dose-time product (DTP, MBq·min) could define as the product of injected activity (MBq) and acquisition time (min). The  $SNR_{norm}$  is normalized to  $SNR_L$ , which is calculated as  $SNR_L$  divided by the square root of the DTP and can be assumed to be independent of the injected activity and acquisition time (Eq. 2) [13]. Therefore,  $SNR_{norm}$  (1/sqrt (MBq·min)) can be regarded as a function of BM-dependent parameters.

$$SNR_{norm} = \frac{SNR_L}{\sqrt{DTP}} \quad (2)$$

Linear fitting was performed with the  $SNR_{norm}$  vs. patient BM. The mean acceptable  $SNR_L$  ( $SNR_{acc}$ ) was obtained by calculating the mean value of  $SNR_L$  from all the images scored with 3 points. Finally, the variable acquisition regimen was determined as follows (Eq. 3):

$$t = \frac{(SNR_{acc}/SNR_{fit})^2}{\text{Injected activity}} \quad (3)$$

where injected activity has a linear correlation with BM and  $SNR_{fit}$  is the determining function of the fit to  $SNR_{norm}$  vs. BM.

The variable-acquisition regimen was validated in a new cohort of 57 patients.  $SNR_L$  was calculated using Eq. 1. Noise can influence the detectability of lesions, which is described as the coefficient of variation (CV):

$$CV = \frac{SD}{SUV_{mean}} \times 100\% \tag{4}$$

The tumor-liver ratio (TLR) and tumor-mediastinal blood pool-ratio (TMR) were calculated by dividing the  $SUV_{max}$  of the lesion by the  $SUV_{mean}$  of the liver and the  $SUV_{max}$  of the lesion by the  $SUV_{mean}$  of the ascending aorta:

$$TLR = \frac{SUV_{max} \text{ of lesion}}{SUV_{mean} \text{ of liver}} \tag{5}$$

$$TMR = \frac{SUV_{max} \text{ of lesion}}{SUV_{mean} \text{ of ascending aorta}} \tag{6}$$

After evaluation of objective and subjective image quality in the validation group, the acquisition time for acceptable image quality was determined. The consistency of acquisition time between the proposed acquisition time regimen and that of the validation group was analyzed.

### Statistical analysis

All statistical analyses were performed using IBM SPSS Statistics Version 26 (IBM Inc., Chicago, IL, USA) and Prism 8 (GraphPad Software Inc., San Diego, California, USA). Data are described as the mean  $\pm$  SD. Differences in quantitative variables were assessed by analysis of variance (ANOVA) with post hoc Bonferroni adjustment for pairwise comparisons. Categorical variables were compared using the chi-square test. Cohen’s kappa analysis of overall image quality was performed to evaluate inter-reader and intrareader agreement. Bland–Altman analysis was applied to determine agreement between the proposed variable acquisition time regimen and validation group data. Results were considered statistically significant if the *p* value was less than 0.05.

### Results

#### Patient characteristics

The characteristics of the two cohorts are displayed in Table 2. A total of 76 NET patients were enrolled. The development cohort consisted of 19 patients (8 male, 11 females, mean age  $51.7 \pm 13.7$  years old, ranging from 30.0 to 74.0 y) scheduled for full activity ( $1.9 \pm 0.2$  MBq/kg, ranging from 1.6 to 2.3 MBq/kg). The validation cohort consisted of 57 patients (36 males and 21 females; mean age,  $53.6 \pm 11.2$  years, ranging from 30.0 to 80.0 y). The injection dose regimen was  $1.0 \pm 0.1$  MBq/kg, ranging from 0.8 to 1.2 MBq/kg. In addition, the mean injected activity was  $120.4 \pm 27.2$  MBq (range:

**Table 2** General characteristics of all participants

Characteristics	Full-activity cohort (N= 19)	Low-activity cohort (N= 57)	$\chi^2/t$	P value
Gender, %			2.60	0.11
Male	8 (42.1)	36 (63.2)		
Female	11 (57.9)	21 (36.8)		
Age, years	$51.7 \pm 13.7$ [30.0–74.0]	$53.6 \pm 11.2$ [30.0–80.0]	0.60	0.55
Weight, kg	$62.3 \pm 11.2$ [45.0–90.0]	$67.7 \pm 13.4$ [42.8–101.8]	1.58	0.12
Height, cm	$165.1 \pm 8.4$ [152.0–183.0]	$166.7 \pm 7.5$ [152.3–180.0]	0.78	0.44
BMI, kg/m <sup>2</sup>	$22.7 \pm 2.8$ [17.3–27.6]	$24.3 \pm 4.1$ [17.1–34.9]	1.58	0.12
Injection activity per weight, MBq/kg	$1.9 \pm 0.2$ [1.6–2.3]	$1.0 \pm 0.1$ [0.8–1.2]	25.83	<0.0001
Injection activity, MBq	$120.4 \pm 27.2$ [88.7–204.9]	$66.9 \pm 11.3$ [41.9–88.0]	12.14	<0.0001
Acquisition time, min	10	10	-	-
Primary tumor location, %				0.72
Pelviabdominal	17 (89.5)	48 (84.2)		
Chest	2 (10.5)	9 (15.8)		
AJCC grade, %				0.55
G1	6 (31.6)	18 (31.6)		
G2	12 (63.2)	29 (50.8)		
G3 or NC	1 (5.3)	10 (17.5)		

Data were as mean  $\pm$  SD [range]

BMI Body mass index, AJCC American Joint Committee on Cancer, NC Neuroendocrine carcinoma

88.7–204.9 MBq) and  $66.9 \pm 11.3$  MBq (range: 41.9–88.0 MBq) for the development and validation cohorts, respectively. Except for injection activity per weight and injection activity, there were no significant differences in sex, age, weight, height, BMI, acquisition time, primary tumor location, or AJCC grade between the two cohorts (all  $p > 0.05$ ).

**Analysis of image quality**

**Development of the variable acquisition time regimen**

There was no significant difference in  $SNR_L$  for D2-D10, though a significant difference in D15s, D30s, D45s, and D1 compared with D10 was observed. The  $SNR_L$  increased with acquisition time, with a significant difference from that at D10 (Fig. 2a and Table 4). The  $SNR_{norm}$ , i.e., the normalized  $SNR_L$ , was not significantly different

among the reconstruction groups (Fig. 2b). The  $SNR_{norm}$  was then fitted with BM using a linear method with a coefficient of determination of 0.63, as illustrated in Fig. 3 ( $R^2 = 0.63$ ). Therefore, the linear fit function was.

$$SNR_{norm} = -0.01 * BM + 1.50 \tag{7}$$

The results of subjective evaluation of image quality are presented in Table 3. The average interreader and intrareader overall image quality showed excellent agreement (all kappa > 0.85). An  $SNR_{acc}$  value of 11.2 was obtained by calculating the average  $SNR_L$  of all PET series with a score of 3 points. Thus, the variable acquisition time regimen can be deduced was  $t(\text{min}) = \frac{(SNR_{acc}/SNR_{fit})^2}{\text{Injected activity}}$ , as follows:

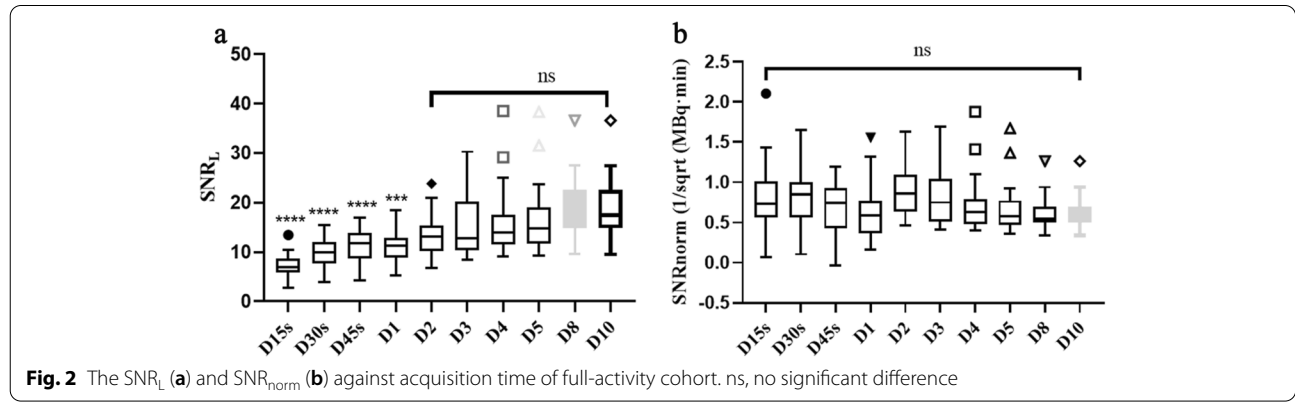


**Fig. 2** The  $SNR_L$  (a) and  $SNR_{norm}$  (b) against acquisition time of full-activity cohort. ns, no significant difference

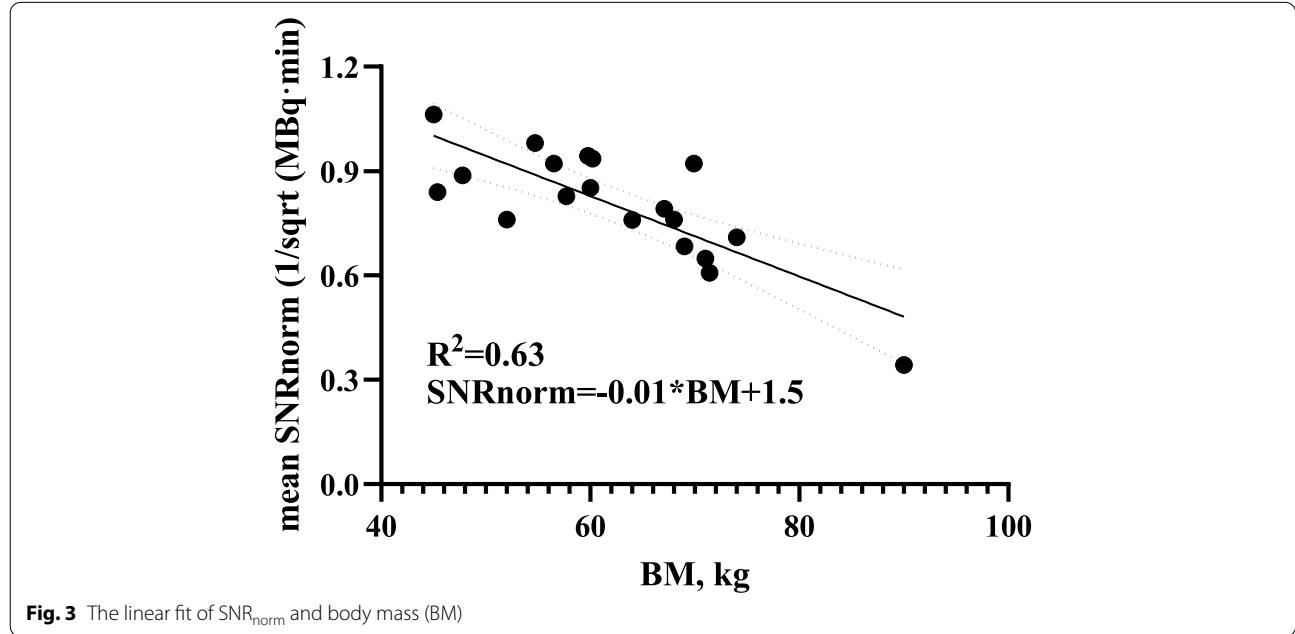


**Fig. 3** The linear fit of  $SNR_{norm}$  and body mass (BM)

**Table 3** Subjective image quality scoring between different reconstruction groups of full-activity cohort

Groups	Mean scores	Inter-reader agreement		Intra-reader agreement			
				Reviewer 1		Reviewer 2	
		kappa	95% CI	kappa	95% CI	kappa	95% CI
D15s	1.34 ± 0.48	0.88	0.83~0.93	0.94	0.85~0.98	0.94	0.85~0.98
D30s	2.24 ± 0.54	0.89	0.84~0.94	0.95	0.88~0.98	0.96	0.90~0.99
D45s	3.13 ± 0.74	0.90	0.86~0.95	0.97	0.92~0.99	1.00	-
D1	3.95 ± 0.61	0.93	0.89~0.95	1.00	-	1.00	-
D2	4.84 ± 0.49	1.00	-	1.00	-	1.00	-
D3	5.00 ± 0.00	1.00	-	1.00	-	1.00	-
D4	5.00 ± 0.00	1.00	-	1.00	-	1.00	-
D5	5.00 ± 0.00	1.00	-	1.00	-	1.00	-
D8	5.00 ± 0.00	1.00	-	1.00	-	1.00	-
D10	5.00 ± 0.00	1.00	-	1.00	-	1.00	-

Mean scores were the mean of two reviewer's score

Cohen's kappa analysis of overall image quality was used to evaluate the inter/intra-reader agreement

Data are presented as the mean ± standard deviation

**Table 4** Semi-quantitative image quality of full-activity cohort

Time	L-SUV <sub>mean</sub>	L-SD	SNR <sub>L</sub>	CV <sub>L</sub>	M-SUV <sub>mean</sub>	M-SD	SNR <sub>M</sub>	CV <sub>M</sub>
D15s	8.97 ± 2.64	1.37 ± 0.65*	7.29 ± 2.36*	15.32 ± 6.23*	0.58 ± 0.23	0.13 ± 0.09*	0.13 ± 0.09*	22.61 ± 10.55*
D30s	8.95 ± 2.62	0.98 ± 0.43*	9.93 ± 2.93*	11.20 ± 4.41*	0.59 ± 0.28	0.09 ± 0.05*	0.09 ± 0.05*	16.07 ± 5.51*
D45s	8.88 ± 2.62	0.89 ± 0.41	11.04 ± 3.52*	10.28 ± 4.39*	0.58 ± 0.27	0.08 ± 0.05	0.08 ± 0.05*	13.28 ± 6.35*
D1	8.62 ± 2.68	0.83 ± 0.33	11.21 ± 3.42*	9.80 ± 3.28*	0.56 ± 0.24	0.06 ± 0.04	0.07 ± 0.05*	12.87 ± 5.86*
D2	8.62 ± 2.61	0.71 ± 0.32	15.39 ± 4.37	8.27 ± 2.79	0.56 ± 0.22	0.05 ± 0.03	0.06 ± 0.04	8.19 ± 5.17
D3	8.63 ± 2.72	0.64 ± 0.26	15.04 ± 6.18	7.61 ± 2.63	0.56 ± 0.21	0.04 ± 0.03	0.05 ± 0.03	8.65 ± 4.16
D4	8.61 ± 2.69	0.62 ± 0.27	15.91 ± 7.65	7.29 ± 2.40	0.55 ± 0.21	0.05 ± 0.03	0.05 ± 0.03	8.10 ± 4.16
D5	8.52 ± 2.64	0.58 ± 0.24	16.66 ± 7.43	6.84 ± 2.18	0.55 ± 0.20	0.05 ± 0.03	0.05 ± 0.03	8.69 ± 4.48
D8	8.55 ± 2.61	0.49 ± 0.19	18.80 ± 6.17	5.82 ± 1.77	0.51 ± 0.21	0.04 ± 0.03	0.04 ± 0.03	7.35 ± 4.56
D10	8.54 ± 2.61	0.49 ± 0.18	19.01 ± 6.08	5.80 ± 1.76	0.52 ± 0.21	0.04 ± 0.03	0.04 ± 0.03	7.32 ± 4.62

Data are presented as the mean ± standard deviation

\*  $p < 0.05$  in Dunnett's multiple comparison test compared with D10. L Liver, M Mediastinal blood pool, SD Standard deviation, SNR<sub>L</sub> Signal noise ratio of the liver, CV Coefficient of variation

**Table 5** Subjective image quality scores between different reconstruction groups of the low-activity cohort

Groups	Mean scores	Inter-reader agreement		Intra-reader agreement			
				Reviewer 1		Reviewer 2	
		kappa	95% CI	kappa	95% CI	kappa	95% CI
R1	1.51 ± 0.50	0.93	0.92~0.94	0.94	0.90~0.97	0.95	0.91~0.97
R2	2.44 ± 0.54	0.90	0.88~0.92	0.98	0.97~0.99	0.95	0.92~0.97
R3	3.44 ± 0.53	0.97	0.96~0.98	0.95	0.91~0.97	0.97	0.95~0.98
R4	4.44 ± 0.57	0.97	0.96~0.98	0.97	0.95~0.98	1.00	-
R5	5.00 ± 0.00	1.00	-	1.00	-	1.00	-
R8	5.00 ± 0.00	1.00	-	1.00	-	1.00	-
R10	5.00 ± 0.00	1.00	-	1.00	-	1.00	-

Mean scores were the mean of two reviewer's score

Cohen's kappa analysis of overall image quality was used to evaluate the inter/intra-reader agreement

Data are presented as the mean ± standard deviation

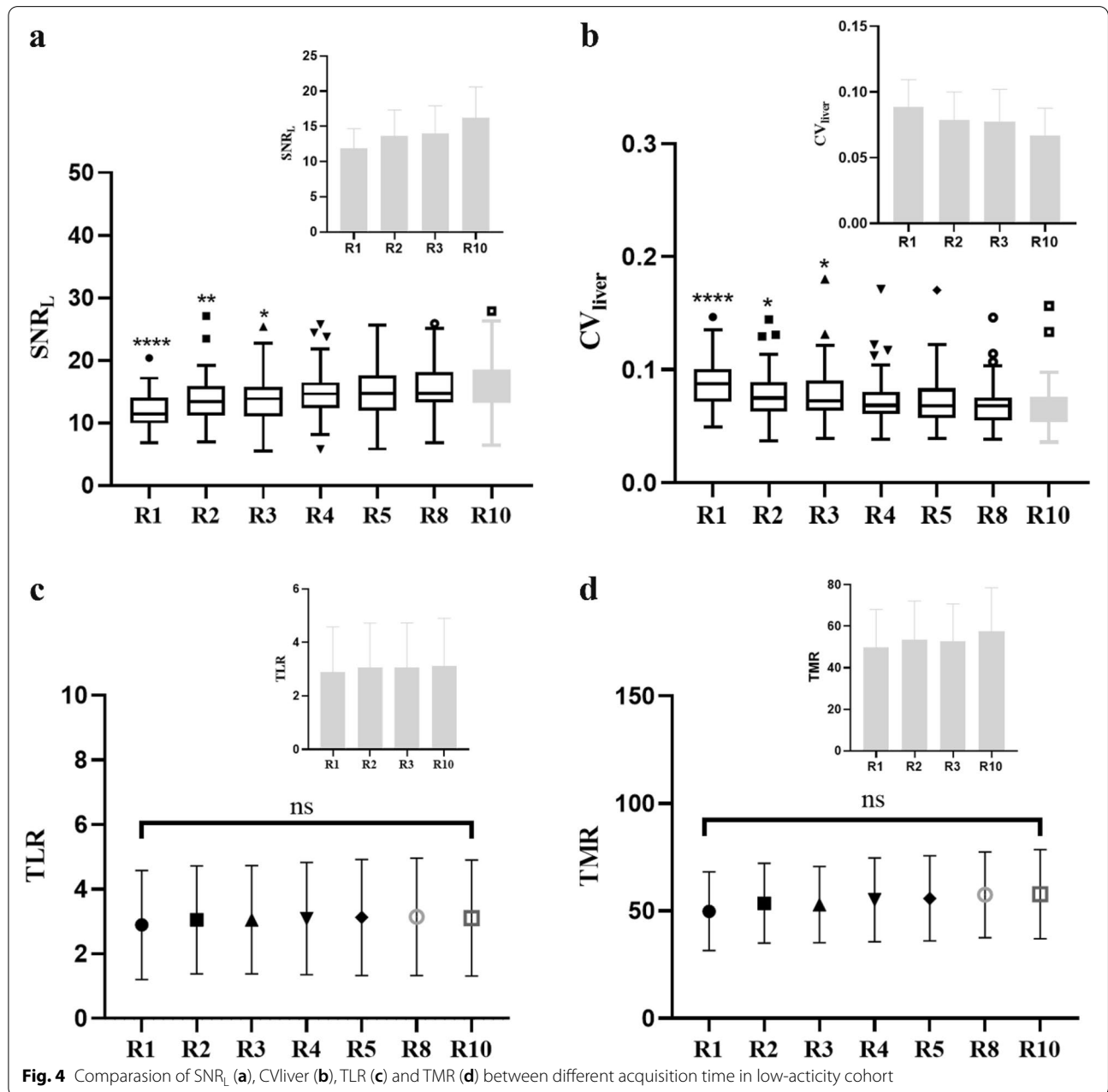
$$t(\text{min}) = \frac{125.40}{a * BM * (-0.01 * BM + 1.50)^2} \quad (8)$$

where  $a$  is the injected activity per weight (MBq/kg). Equation 8 is suitable for body mass less than 150 kg. The semiquantitative parameters are summarized in detail in Table 4. There were no differences in the  $SUV_{\text{mean}}$  of the liver or the  $SUV_{\text{mean}}$  of the mediastinal blood pool among the reconstruction groups (all  $p > 0.05$ ). Compared with D10, the liver SD and mediastinal blood pool were only decreased in D15s and D30s ( $p < 0.05$ ). Furthermore, the liver SNR, mediastinal blood pool SNR, liver CV, and

mediastinal blood pool CV progressively differed for D15s, D30s, D45s, and D1 ( $p < 0.05$ ); there was no difference from D2 to D10 (all  $p > 0.05$ ).

**Analysis of image quality in the validation cohort**

Objective and subjective image quality were evaluated in the validation cohort (the low activity:  $1.0 \pm 0.1$  MBq/kg). Table 5 provides an overview of the subjective scores for all reconstruction groups. The average overall image quality scores in the R1 and R2 groups were less than 3 and were considered to be non-diagnostic images. All images with a 3 min or longer





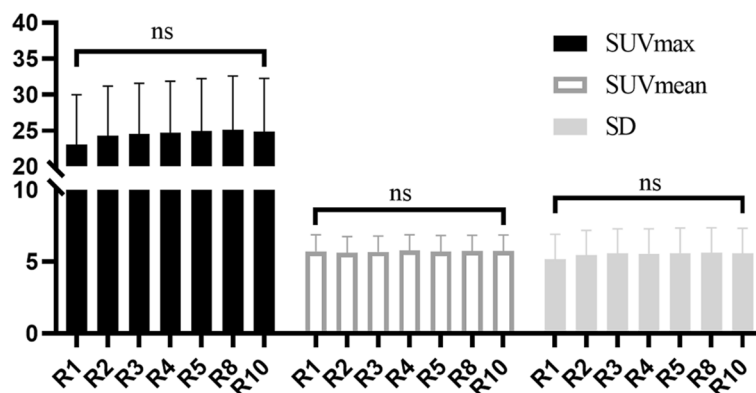


**Fig. 5** The SUVmax, SUVmean and SD of lesions between all reconstruction groups in low-activity cohort

acquisition time were viewed as diagnostic images (score  $\geq 3$ ). The interreader and intrareader agreement of the overall image quality of all PET series indicated excellent agreement, with kappa values over 0.85. As indicated in Fig. 4a, the  $SNR_L$  was significantly lower in the R1, R2, and R3 groups than in the R10 group, though R4, R5, R8, and R10 showed no significant differences ( $p < 0.05$ ). The CV is presented against acquisition time in Fig. 4b, and it decreased significantly with reconstruction time in R1, R2, R3 compared with R10. However, there was no obvious difference for R4, R5, R8, and R10. There were also no significant discrepancies in the lesion  $SUV_{max}$ ,  $SUV_{mean}$ , SD, TMR, or TBR among the series of reconstructions (all  $p > 0.05$ , Figs. 4c-d and 5).

Compared with D2 of the development cohort, R4 obtained equal values of  $SUV_{max}$  and  $SUV_{mean}$  for the liver, blood pool, and lesions (shown in Table 6). The CV of the liver and blood pool also showed equal. The TLR and TMR of R2 were comparable to those of R10. Referenced as PET images of R10, 90 SSTR-positive lesions were identified. Lesions were detected in the liver (38, 42.2%), bone (18, 20.0%), lymph nodes (15, 16.7%), gastrointestinal tract (10, 11.1%), pancreas (5, 5.6%), breast (2, 2.2%), and mediastinum (2, 2.2%), and all of these lesions were clearly found in the R1-R10 groups (100%).

**Agreement of optimal acquisition time between two methods**

Figure 6A shows the optimal acquisition time in the validation cohort, with an average time of  $2.99 \pm 0.91$  min, ranging from 2.18 to 6.35 min, calculated by the regime of Eq. 8. The agreement between proposed and subjective optimal time was analyzed by Bland–Altman plots (Fig. 6b). It showed good agreement between the

proposed regimen and the validation patient cohort. The mean bias between the proposed regimen and the validation patient cohort was -0.16 min, with 95% acceptable limits of -0.79 min and 0.48 min. A typical case is presented in Fig. 7.

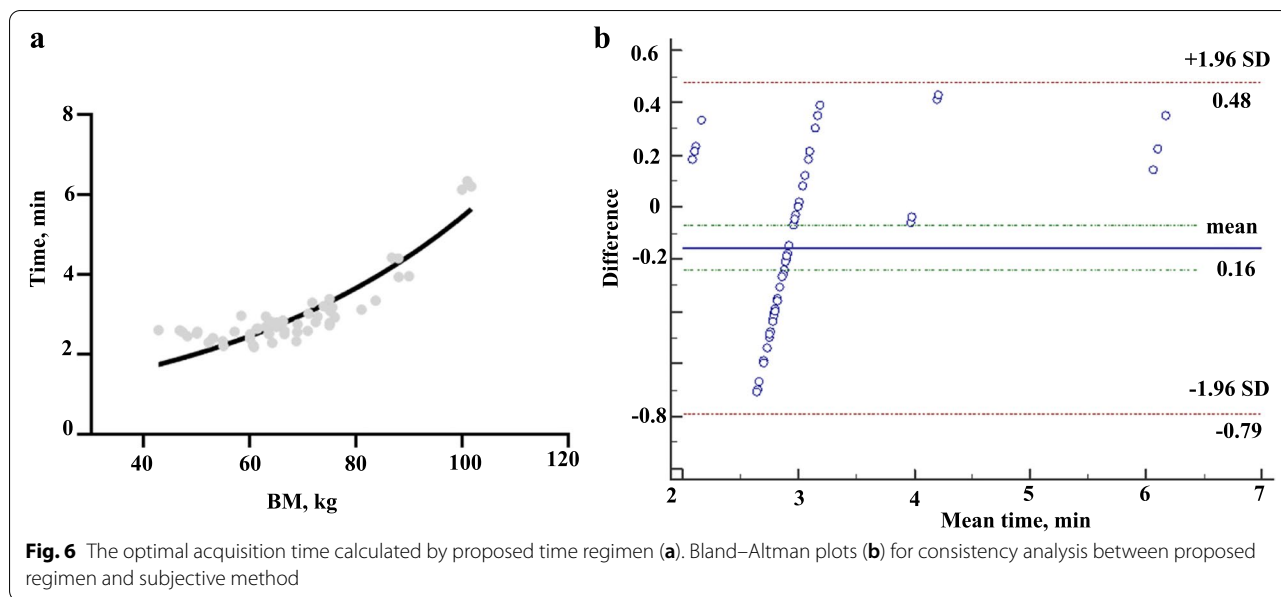
**Discussion**

The 2017 European Association of Nuclear Medicine (EANM) procedure guidelines recommend that the administered activity of  $^{68}Ga$ -DOTA-conjugated peptide ranges from 100 to 200 MBq, varying based on the PET system and patient size [17]. Although that recommendation provides a reference for clinical practice, such a broad injection range creates certain challenges with respect to the comparability and repeatability of images. In previous research, we established a convenient

**Table 6** Objective image quality parameters in D2 and R4 group

Parameters	D2	R4	P value
Image quality score	4.84 ± 0.49	4.44 ± 0.57	0.49
Liver SUVmax	10.2 ± 3.4 [6.1–20.9]	9.6 ± 2.4 [4.3–15.3]	0.51
Liver SUVmean	8.6 ± 2.7 [5.7–17.2]	8.4 ± 2.1 [3.7–12.7]	0.85
Liver SNR	13.4 ± 4.4 [6.9–23.8]	14.7 ± 3.9 [5.8–25.4]	0.41
CV <sub>liver</sub> , %	8.3 ± 0.3 [4.2–14.6]	7.3 ± 2.2 [3.8–17.1]	0.13
Blood pool SUVmax	0.7 ± 0.3 [0.4–1.3]	0.5 ± 0.2 [0.2–1.4]	0.08
Blood pool SUVmean	0.6 ± 0.2 [0.3–1.1]	0.5 ± 0.2 [0.2–1.1]	0.14
CV <sub>blood</sub> , %	10.2 ± 5.2 [4.8–22.0]	9.3 ± 3.5 [2.9–27.7]	0.41
Lesions SUVmax	19.4 ± 17.1 [1.6–43.2]	24.7 ± 40.5 [1.6–232.1]	0.73
TLR	3.1 ± 4.6 [0.2–26.5]	3.1 ± 5.0 [0.2–28.7]	0.58
TMR	35.8 ± 42.8 [4.7–130.9]	55.2 ± 54.0 [4.1–209.1]	0.37

CV<sub>liver</sub> Coefficient of variation of liver, CV<sub>blood</sub> Coefficient of variation of mediastinal blood pool, TLR Tumor-liver -ratio; TMR Tumor-mediastinal blood pool-ratio  
Data were described as mean ± SD [range]



patient-specific injection regimen of  $^{18}\text{F}$ -FDG for repeatable and constant imaging. Thus, considering the influence of the total-body PET system and body mass on image quality, the present study proposes a personal variable acquisition time regimen to gain constant image quality and avoid extending acquisition time based on objective and subjective image quality evaluation in the development of  $^{68}\text{Ga}$ -DOTATATE PET/CT imaging. Next, the variable acquisition time regimen was validated and assessed for agreement with objective and subjective image quality evaluations in a validation cohort. The method we designed for a variable acquisition regimen might be instructive for other PET systems.

Image quality is commonly evaluated by the metric SNR or noise equivalent count rate (NECR). The SNR is calculated as the value of the square root of the product of system sensitivity, injected activity, and acquisition time [13], whereas the NECR is calculated as the ratio of the square of the true events to the total of true events, random events, and scatter coincidences [18]. A constant value of SNR and NECR can overcome the limitation of patient-specific attenuation to render uniform image quality. To achieve a constant image, acquisition time should vary from different patient size. For example, a typical patient with 100 kg should scan more time than a patient with 50 kg to achieve target SNR. One patient scanning by a related lower sensitivity detector should prolong acquiring time than by higher sensitive detector. In addition, to achieve target SNR, low activity of tracer should have longer scanning time than high activity. In developing cohort, the  $\text{SNR}_L$  increased with increasing acquisition time within 1 min

(Fig. 2a). The  $\text{SNR}_{\text{norm}}$  showed a strong correlation with body mass (less than 150 kg) with a determination coefficient (R square) of 0.63, slightly lower than that in a previous study [13]. We speculate that the range of body mass and the sample size might have contributed to this difference.

Based on the excellent intra- and inter-agreement agreement (all kappa > 0.85), the mean threshold  $\text{SNR}_L$  was 11.2 for acceptable image quality of  $^{68}\text{Ga}$ -DOTATATE total-body PET/CT. Compared with  $^{18}\text{F}$ -FDG images we previously analyzed, the threshold SNR of 14.0 was slightly higher. The difference was consistent with a previous study in which the acceptable  $\text{SNR}_L$  was 6.2 for whole-body  $^{68}\text{Ga}$ -DOTATATE PET/CT, but  $^{18}\text{F}$ -FDG studies have revealed a higher SNR of 10 [19]. Compared with  $^{18}\text{F}$ -FDG with liver SUVmean of 2.6, the accumulation degree of  $^{68}\text{Ga}$ -DOTATATE in liver was higher with liver SUVmean of 8.4 [11]. We hypothesize that difference might be related to the percentage of biological distribution in the liver. In addition, the coefficient of variation, representing image noise, is recommended to be 15% as a reference maximum noise level for clinical  $^{18}\text{F}$ -FDG PET image interpretation [20]. In the present study, both the CV of D2 in the development cohort and R4 in the validation cohort were less than 10%. A recent study [9] showed that 5.5 times noise reduction of a 194-cm FOV PET compared to a 30-cm FOV digital PET with the same total examination time for scanning a 2-m-long phantom, and the noise reduction became 1.5 times when the same acquisition time per bed was performed.

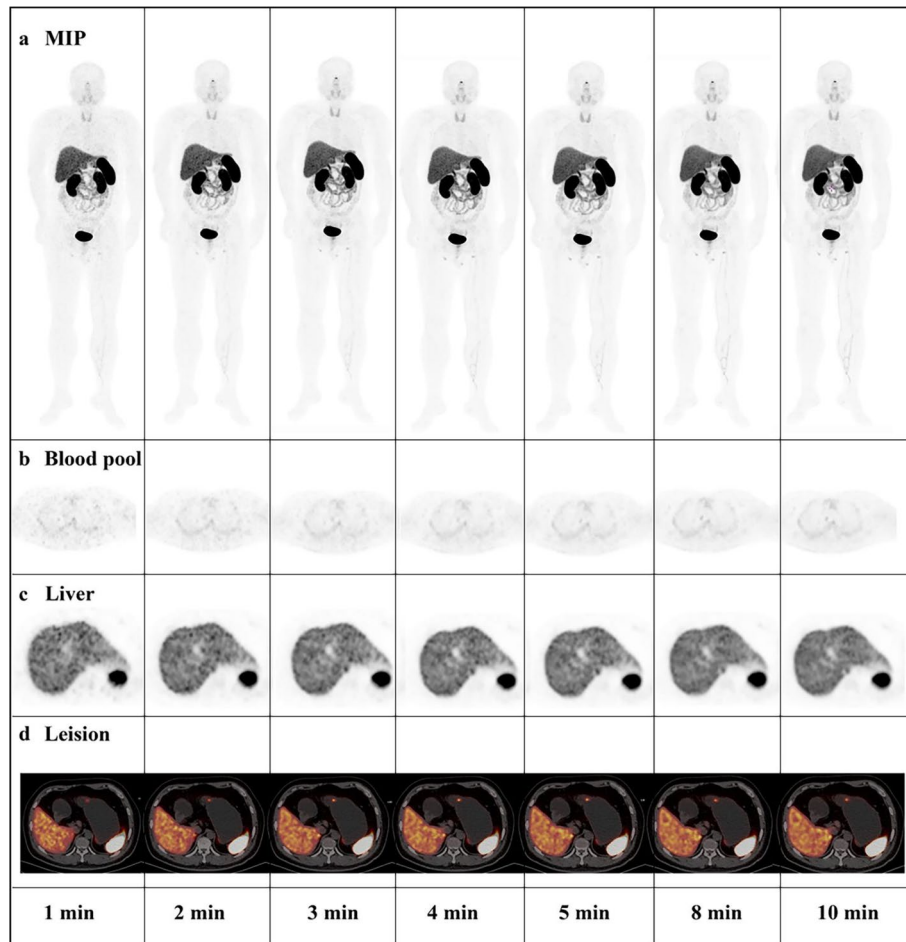


**Fig. 7** A-39-year-old man of 80 kg confirmed as G2 grade NET by gastroscopie guide biopsy. Imaging of MIP (**a**) showed avid  $^{68}\text{Ga}$ -DOTATATE in gastric body for R1-R10. The axial PET images showed corresponding mediastinal blood pool (**b**) and liver (**c**). The lesion in gastric body was clearly displayed in all reconstruction times. Based on the variable-acquisition time regimen, the threshold time was 2.4 min, and the subjective score was 3.0 min

In the validation cohort, all 90 lesions were detected in all acquisition time PET images of all subgroups. The higher percentage of G1 and G2 patients with marked SSTR expression (18/19 for the development cohort and 47/57 for the validation cohort) than G3 or NEC patients enrolled in this study might lead to bias in the results. Based on the proposed variable time regimen, the mean time was  $2.99 \pm 0.91$  min, ranging from 2.18 to 6.35 min. Compared to the fixed acquisition protocol of 10 min, the mean acquisition time decreased by 70.1%, ranging from 36.5% to 78.2%. The variable acquisition time regimen based on a constant  $\text{SNR}_L$  of 11.2 of total-body scan can eliminate the influence of BM, and provide more consistent image quality.

In this study, SNR was selected for evaluation of image quality because there was relatively homogeneous uptake of  $^{68}\text{Ga}$ -DOTATATE by the liver, which was easily

influenced by several circumstances. Previous studies have found less uptake of  $^{68}\text{Ga}$ -DOTATATE by the liver, spleen, and thyroid after treatment initiation in patients with than without somatostatin analog treatment [21]. One prospective study performed  $^{68}\text{Ga}$ -DOTATATE imaging one day before and one day after injection of lanreotide, and no evidence of decreased uptake in the tumor, but a higher tumor-to-liver ratio, was obtained [22]. To avoid the influence of treatment, our study excluded 6 patients with continuous treatment with octreotide and one patient with high-intensity focused ultrasound in the liver within 1 week. Additionally, the dynamic distribution between the development cohort regimen and low-activity regimen exhibited equivalent trends for the liver, pancreas, kidney, and spleen over time, which might eliminate the influence of different doses on biological distribution (Fig. S2).

In addition, the image quality could also be improved using the reconstructed method of PSF and TOF. Previous study reported that the TOF could obtain more contract information than that without TOF information [23]. Although the image reconstructed with PSF correction slowed the iterative convergence, it could provide a more uniform background and increased SNR than that without PSF correction. Previous study showed that the sufficient image quality could be acquired for low activity objects and a shorter acquisition time when the image constructed by PSF and TOF [24]. In this study, the sufficient image quality might be contributed by the combination of ultra-high sensitivity of total body detector and the image reconstructed by TOF and PSF.

The findings of this study have to be considered in light of several limitations. First, the variable acquisition time regimen was established based on retrospective image reconstructions for 19 full-activity cases. The small sample size may result in confounding bias that may influence the reliability of the proposed regimen. Second, further investigation focusing on more organ SNRs, such as the spleen, kidney and additional metrics for image quality are needed. Third, we provide a method to realize personalized duration time; however, the acquisition time regimen was established only on total body PET. Thus, the proposed method should be referred to and rebuilt for other PET systems according to those characteristics.

## Conclusion

A BM-specific acquisition time regimen was proposed and validated in patients with NETs on  $^{68}\text{Ga}$ -DOTA-TATE total-body PET/CT imaging. Based on the proposed regimen, the homogenous image quality with reasonable acquisition time was available for a constant level, independent of body mass.

## Abbreviations

BM: Body mass; PET/CT: Positron emission tomography/computed tomography; OSEM: Ordered subsets expectation maximization; TOF: Time of flight; PSF: Point spread function; SD: Standard deviation; SNR: Signal to noise ratio; SUVmax: Maximum standard uptake value; SUVmean: Mean standard uptake value; ROI: Region of interest; NECR: Noise equivalent count rate; CV: Coefficient of variation; SSTR: Somatostatin receptor; EANM: European Association of Nuclear Medicine; TLR: Tumor-liver ratio; TMR: Tumor-mediastinal blood pool-ratio.

## Supplementary Information

The online version contains supplementary material available at <https://doi.org/10.1186/s40644-022-00517-8>.

**Additional file 1: Supplement Fig. 1.** Diagram of basic acquisition protocol covering one bed position. AC = attenuation correction CT. **Supplement Fig. 2.** Time activity curve showed the biological distribution in liver (ROI1), spleen (ROI2), kidney (ROI3) and pancreas (ROI4) have same trends in the half-activity (a) and the full-activity (b). **Supplement Table 1.**

Consistency training for 35 standard images interpreting between two physicians.

## Acknowledgements

Throughout the writing of this paper, I have received a great deal of support and assistance. I would like to acknowledge Professor Hongcheng Shi and Dengfeng Cheng for inspiring my interest in the development of innovative technologies.

## Authors' contributions

Jie Xiao was involved in the statistical analysis and manuscript writing. Haojun Yu contributed to the data acquisition and reconstructions. Jie Xiao and Xiuli Sui contributed to the data analyses and image interpretation. Thanks are due to Yanyan Cao for checking the authenticity of all measurements and clinical data. Thanks for valuable discussion to Yiqiu Zhang and Pengcheng Hu. Qingyu Lin and Yanzhao Zhao were responsible for the pharmaceutical synthesis and quality control. Hongcheng Shi and Dengfeng Cheng designed the study and contributed to editing and reviewing the manuscript. The author(s) read and approved the final manuscript.

## Funding

This study is supported by the Three-year Action Plan of Clinical Skills and Innovation of Shanghai Hospital Development Center (Grant number: SHDC-2020CR3079B), Science and Technology Committee of Shanghai Municipality (Grant number: 20DZ2201800), Special Fund for Clinical Research, Young Program of Zhongshan Hospital of Fudan University (Grant number: 2019ZSYQ28, 2020ZSLC63), Young Program of Zhongshan Hospital and Shanghai "Rising Stars of Medical Talent"-Youth Development Program (Grant number: HWJRS2019-720), Shanghai Municipal Key Clinical Specialty Project (Grant number: SHSLCZDZK03401), and Next-generation information infrastructure construction project from Shanghai Municipal Commission of Economy and Informatization (Grant number: 201901014).

## Availability of data and materials

Not applicable.

## Declarations

### Ethics approval and consent to participate

All procedures performed in studies involving human participants were in accordance with the ethical standards of the institutional and/or national research committee and with the 1964 Helsinki declaration and its later amendments or comparable ethical standards.

### Consent for publication

All individual person's data in this study have consent to publish. All authors read and approved the final manuscript.

### Competing interests

We declare that none of the authors has any conflicts of interest.

### Author details

<sup>1</sup>Department of Nuclear Medicine, Zhongshan Hospital, Fudan University, 180 Fenglin Road, 200032 Shanghai, P.R. China. <sup>2</sup>Institute of Nuclear Medicine, Fudan University, Shanghai 200032, China. <sup>3</sup>Shanghai Institute of Medical Imaging, Shanghai 200032, China. <sup>4</sup>Collaborative Innovation Center for Molecular Imaging Precision Medicine, Shanxi Medical University, Taiyuan, Shanxi 030001, People's Republic of China.

Received: 17 July 2022 Accepted: 19 December 2022

Published online: 29 December 2022

## References

1. Dasari A, Shen C, Halperin D, Zhao B, Zhou S, Xu Y, et al. Trends in the incidence, prevalence, and survival outcomes in patients

- with neuroendocrine tumors in the United States. *JAMA Oncol.* 2017;3(10):1335–42.
2. Reubi JC, Waser B. Concomitant expression of several peptide receptors in neuroendocrine tumours: molecular basis for in vivo multireceptor tumour targeting. *Eur J Nucl Med Mol Imaging.* 2003;30(5):781–93.
  3. Reubi JC, Schär JC, Waser B, Wenger S, Heppeler A, Schmitt JS, et al. Affinity profiles for human somatostatin receptor subtypes SST1–SST5 of somatostatin radiotracers selected for scintigraphic and radiotherapeutic use. *Eur J Nucl Med Mol Imaging.* 2000;27(3):273–82.
  4. Antunes P, Ginj M, Zhang H, Waser B, Baum RP, Reubi JC, et al. Are radiogallium-labelled DOTA-conjugated somatostatin analogues superior to those labelled with other radiometals? *Eur J Nucl Med Mol Imaging.* 2007;34(7):982–93.
  5. Miwa K, Umeda T, Murata T, Wagatsuma K, Miyaji N, Terauchi T, et al. Evaluation of scatter limitation correction: a new method of correcting photopenic artifacts caused by patient motion during whole-body PET/CT imaging. *Nucl Med Commun.* 2016;37(2):147–54.
  6. Du J, Ariño-Estrada G, Bai X, Cherry SR. Performance comparison of dual-ended readout depth-encoding PET detectors based on BGO and LYSO crystals. *Phys Med Biol.* 2020;65(23):10.
  7. Badawi RD, Shi H, Hu P, Chen S, Xu T, Price PM, et al. First human imaging studies with the EXPLORER total-body PET scanner. *J Nucl Med.* 2019;60(3):299–303.
  8. Tan H, Sui X, Yin H, Yu H, Gu Y, Chen S, et al. Total-body PET/CT using half-dose FDG and compared with conventional PET/CT using full-dose FDG in lung cancer. *Eur J Nucl Med Mol Imaging.* 2021;48(6):1966–75.
  9. Liu G, Xu H, Hu P, Tan H, Zhang Y, Yu H, et al. Kinetic metrics of 18F-FDG in normal human organs identified by systematic dynamic total-body positron emission tomography. *Eur J Nucl Med Mol Imaging.* 2021;48(8):2363–72.
  10. Zhang YQ, Hu PC, Wu RZ, Gu YS, Chen SG, Yu HJ, et al. The image quality, lesion detectability, and acquisition time of 18F-FDG total-body PET/CT in oncological patients. *Eur J Nucl Med Mol Imaging.* 2020;47(11):2507–15.
  11. Xiao J, Yu H, Sui X, Hu Y, Cao Y, Liu G, et al. Can the BMI-based dose regimen be used to reduce injection activity and to obtain a constant image quality in oncological patients by 18F-FDG total-body PET/CT imaging? *Eur J Nucl Med Mol Imaging.* 2021;49(1):269–78.
  12. Namías M, Jeraj R. Patient and scanner-specific variable acquisition times for whole-body PET/CT imaging. *Phys Med Biol.* 2019;64(20):205013.
  13. Cox CPW, Segbers M, Graven LH, Brabander T, van Assema DME. Standardized image quality for 68Ga-DOTA-TATE PET/CT. *EJNMMI Res.* 2020;10(1):27–36.
  14. Woltering EA, Bergsland EK, Beyer DT. Neuroendocrine tumors of the stomach. American Joint Committee on Cancer 2017. In: Amin MB editor. *AJCC Cancer Staging Manual.* Eighth Edition. Springer; 2017. pp. 351–59. [https://doi.org/10.1007/978-3-319-40618-3\\_30](https://doi.org/10.1007/978-3-319-40618-3_30).
  15. Tworowska I, Ranganathan D, Thamake S, Delpassand E, Mojtahedi A, Schultz MK, et al. Radiosynthesis of clinical doses of 68Ga-DOTATATE (Galiomedix™) and validation of organic-matrix-based 68Ge/68Ga generators. *Nucl Med Biol.* 2016;43(1):19–26.
  16. de Groot EH, Post N, Boellaard R, Wagenaar NR, Willemsen AT, van Dalen JA. Optimized dose regimen for whole-body FDG-PET imaging. *EJNMMI Res.* 2013;3(1):63–73.
  17. Bozkurt MF, Virgolini I, Balogova S, Beheshti M, Rubello D, Decristoforo C, et al. Guideline for PET/CT imaging of neuroendocrine neoplasms with 68Ga-DOTA-conjugated somatostatin receptor targeting peptides and 18F-DOPA. *Eur J Nucl Med Mol Imaging.* 2017;44(9):1588–601.
  18. Rana N, Kaur M, Singh H, Mittal BR. Dose Optimization in 18F-FDG PET Based on Noise-Equivalent Count Rate Measurement and Image Quality Assessment. *J Nucl Med Technol.* 2021;49(1):49–53.
  19. Mizuta T, Senda M, Okamura T, Kitamura K, Inaoka Y, Takahashi M, et al. NEC density and liver ROI S/N ratio for image quality control of whole-body FDG-PET scans: comparison with visual assessment. *Mol Imaging Biol.* 2009;11(6):480–6.
  20. Gnesin S, Kieffer C, Zeimpekis K, Papazyan JP, Guignard R, Prior JO, et al. Phantom-based image quality assessment of clinical 18F-FDG protocols in digital PET/CT and comparison to conventional PMT-based PET/CT. *EJNMMI Phys.* 2020;7(1):1–16.
  21. Gálne A, Almquist H, Almquist M, Hindorf C, Ohlsson T, Nordenström E, et al. A prospective observational study to evaluate the effects of long-acting somatostatin analogs on 68Ga-DOTATATE uptake in patients with neuroendocrine tumors. *J Nucl Med.* 2019;60(12):1717–23.
  22. Aalbersberg EA, de Wit-van der Veen BJ, Versleijen MWJ, et al. Influence of lanreotide on uptake of 68Ga-DOTATATE in patients with neuroendocrine tumours: a prospective intra-patient evaluation. *Eur J Nucl Med Mol Imaging.* 2019;46(3):696–703.
  23. Ptáček J, Karhan P, Fiala P. Optimal reconstruction matrix and PET image filtration for point-spread function and time-of-flight reconstruction - A phantom study. *Phys Med.* 2017;39:95–9.
  24. Rogasch JM, Suleiman S, Hofheinz F, Bluemel S, Lukas M, Amthauer H, et al. Reconstructed spatial resolution and contrast recovery with Bayesian penalized likelihood reconstruction (Q.Clear) for FDG-PET compared to time-of-flight (TOF) with point spread function (PSF). *EJNMMI Phys.* 2020;7(1):2.

## Publisher's Note

Springer Nature remains neutral with regard to jurisdictional claims in published maps and institutional affiliations.

Ready to submit your research? Choose BMC and benefit from:

- fast, convenient online submission
- thorough peer review by experienced researchers in your field
- rapid publication on acceptance
- support for research data, including large and complex data types
- gold Open Access which fosters wider collaboration and increased citations
- maximum visibility for your research: over 100M website views per year

At BMC, research is always in progress.

Learn more [biomedcentral.com/submissions](https://biomedcentral.com/submissions)

